Earth and Planetary Science Letters 471 (2017) 117–124

Contents lists available at ScienceDirect

Earth and Planetary Science Letters

www.elsevier.com/locate/epsl

Uppermost mantle and crustal structure at Tristan da Cunha derived from ambient seismic noise

T. Ryberg [a,*], W.H. Geissler [b], W. Jokat [b,c], S. Pandey [b,d]

[a] Helmholtz Centre Potsdam GFZ German Research Centre for Geosciences, Telegrafenberg, Potsdam, Telegrafenberg, 14473 Potsdam, Germany
[b] Alfred Wegener Institute Helmholtz Centre for Polar and Marine Research, Am Handelshafen 12, 27570 Bremerhaven, Germany
[c] University of Bremen, Department of Geoscience, 28359 Bremen, Germany
[d] Shillong Geophysical Research Centre, IIG, Wilton Hall Estate, Upper Shillong 793005, India

A R T I C L E I N F O

Article history:
Received 21 February 2017
Received in revised form 26 April 2017
Accepted 28 April 2017
Available online 19 May 2017
Editor: P. Shearer

Keywords:
ambient seismic noise
surface wave tomography
hotspot volcanism
South Atlantic opening
Tristan da Cunha

A B S T R A C T

According to classical plume theory, the Tristan da Cunha hotspot, located ∼400 km east off the Mid-Atlantic Ridge, is thought to have played a major role in the rifting while creating an aseismic Walvis Ridge during and after the breakup of the South Atlantic margins. Volcanic activity on the Tristan da Cunha Island shows that the hotspot might still be there influencing the upper mantle and crustal structure. In this study we present ambient noise data from 24 broadband OBS around Tristan da Cunha and a seismic station on Nightingale Island, which provide first constraints on the crustal and uppermost mantle structure around the island. By combining ambient noise techniques, dispersion curve analysis of Rayleigh waves, 2D tomographic inversion of travel times and 3D depth inversion of dispersion data we derived a 3D V_S velocity model around the archipelago of Tristan da Cunha. The model shows an isolated, vertically sharp bounded thickened and modified crust beneath the islands surrounded by thin oceanic crust (<5 km). The velocity anomaly shows a typical volcanic structure with a shallow high velocity body and a low velocity root reaching into the upper mantle, which we interpret as shallow solidified magmatic material and volcanic feeding system/magmatic underplating, respectively. The observed simple and localized volcanic structure, embedded in a rather homogeneous crust and upper mantle indicates only minor and very localized magmatic overprinting of the existing lithosphere by the Tristan da Cunha hotspot. The uppermost mantle S wave velocity beneath nearby seamounts and to the SW of the islands is also slow and could indicate a thermal influence from a deeper source, whereas the Tristan da Cunha Fracture Zone shows no signs of modification.

1. Introduction

Tristan da Cunha is located in the South Atlantic approximately 400 km to the east of the Mid-Atlantic Ridge (Fig. 1). It represents the southwestern termination of the aseismic Walvis Ridge, which is believed to represent one of the classical hot spot tracks (O'Connor and Duncan, 1990) and might mark the recent position of a mantle plume (Morgan, 1971; Courtillot et al., 2003). There is ongoing discussion, if the Tristan da Cunha Mantle Plume played a major role in driving the break-up of the South Atlantic ∼132 Ma (Fromm et al., 2015; Ryberg et al., 2015). The search for any geophysical/thermal anomalies within the crust and uppermost mantle beneath Tristan da Cunha was the starting point of a multi-disciplinary geophysical experiment by acquiring passive marine electromagnetic, seismic, and bathymetric data within the framework of the SPP1375 **S**outh **A**tlantic **M**argin **P**rocesses and **L**inks with onshore **E**volution (SAMPLE) funded by the German Science foundation. The experiment included two ship expeditions on-board the German R/V MARIA S. MERIAN in 2012 and 2013. First we intended to image a likely anomalous lithosphere structure beneath the active ocean island volcano. A second objective was to find constraints on potential interactions of the assumed mantle plume with the nearby mid-ocean ridge, as it is suggested by geochemical data (Schilling et al., 1985), as well as the potential influence of the nearby Tristan da Cunha Fracture Zone (TDCFZ).

In general, any strong interaction of a thermal anomaly with melting at the mid-ocean ridge should result in the production of thicker oceanic crust (White et al., 1992). Due to the absence of deep seismic refraction data we used here Rayleigh surface waves recovered from ambient ocean noise to study the lateral variations of the crust in the vicinity of Tristan da Cunha. The data processing methods consisted of several steps: ambient noise analysis, 2D

* Corresponding author.
E-mail address: trond@gfz-potsdam.de (T. Ryberg).

http://dx.doi.org/10.1016/j.epsl.2017.04.049
0012-821X/

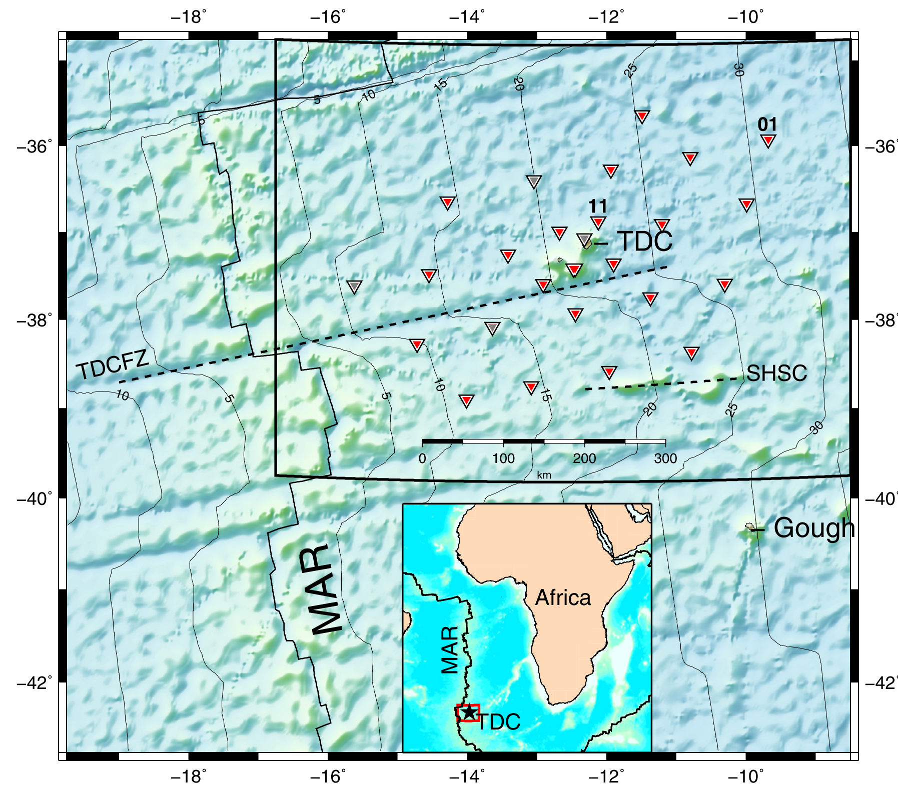

Fig. 1. Map of study region with 24 ocean bottom seismic broad band stations and 2 land stations at Tristan da Cunha islands (TDC) indicated by red triangles (no data for gray stations). The volcanic islands are located ∼400 km E of the Mid-Atlantic Ridge (MAR). The black box indicates the actual area of velocity inversion. Sea-floor ages are from Müller et al. (2008). The dashed lines show the location of the Speedwell-Hercules Seamount Chain (SHSC) and Tristan da Cunha Fault Zone (TDCFZ). (For interpretation of the references to color in this figure, the reader is referred to the web version of this article.)

Rayleigh wave tomography followed by a depth conversion according to Ryberg et al. (2016), now adapted and firstly applied to ocean bottom data.

Tristan da Cunha is part of a remote group of active volcanic islands in the South Atlantic, consisting of the islands of Tristan da Cunha, Nightingale and Inaccessible. The southernmost volcano is Gough Island located about 400 km further south. The largest island, Tristan da Cunha is still volcanically active (Fig. 1). The last eruption happened here in 1961. With an elevation of more than 2000 m it rises >5.5 km above the adjacent sea floor. In 2004, there are reports on a submarine eruption south of the island (e.g., O'Mongain et al., 2007). Tristan da Cunha is suggested to represent a classical example of the active end of a hotspot track, with a characteristic age progression starting at ∼132 Ma at the Etendeka flood basalt province on the African continent (Hicks et al., 2012; O'Connor and Duncan, 1990). On the conjugate South American plate, the Paraná continental flood basalts and the submarine Rio Grande Rise also document the magmatic history (∼132–70 Ma) of the Tristan–Gough hotspot track system. One characteristic of the young end of the hotspot track is the wide scattering of seamounts, which actually forms multiple tracks, as it is documented also in geochemistry of the volcanic rocks (Rohde et al., 2013). The Speedwell-Hercules Seamount Chain (Fig. 1, SHSC) is located south of the Tristan da Cunha Fracture Zone at the southern periphery of our seismological network.

Only recently, new geophysical (Baba et al., 2016; Geissler et al., in press; Schloemer et al., 2017) and petrological data (Weit et al., 2016) were published which help to better constrain the underlying causes for the magmatic activity in this intra-plate setting. Whereas Baba et al. (2016) did not find evidence from magnetotelluric data for the existence of a mantle plume beneath the study area, Schloemer et al. (2017) imaged a low P-wave velocity conduit within the upper mantle, which could represent the uppermost part of a weak mantle plume. Geissler et al. (in press) studied the thicknesses of the crust, lithosphere and mantle transition zone by means of receiver functions. Due to very noisy and therefore questionable observations of converted phases from the mantle transition zone to the south of Tristan da Cunha, Geissler et al. (in press) only found weak indications for a mantle plume at mid-mantle depths. Weit et al. (2016) studied the magmatic system beneath Tristan da Cunha analyzing thermo-barometric data and found rock crystallization depths of 6–10 and 24–36 km, representing potential levels of magmatic intrusions into the crust and uppermost mantle. Furthermore, Weit et al. (2016) modeled the origin of the associated magmas in a depth range of ∼60 km to ∼80–100 km.

2. Data acquisition

Between February 2012 and January 2013 a network of 24 broadband ocean-bottom seismometers (OBS) was in operation around the volcanic archipelago of Tristan da Cunha, complemented by a temporary land station on Nightingale Island (Fig. 1). The permanent station TRIS (Global Seismograph Network) failed to record data during the duration of our experiment. The seismological network had a size of approximately 500 km by 350 km. The OBS were equipped with Güralp CMG-40T broadband seismometer (60 s) incorporated in a titanium pressure housing, a hydrophone, and a GEOLON MCS (**M**arine **C**ompact **S**eismocorder) data logger. Each sensor channel was sampled at 50 Hz (2 broad band OBS at 100 Hz) up to 350 days, preamplifier gain of the hydrophone channel was 4 and 1 for the three seismometer components. The noise level and spectral content of the OBS and land station recordings are typical for oceanic environments with dominating signal periods around 5 s (Fig. S1).

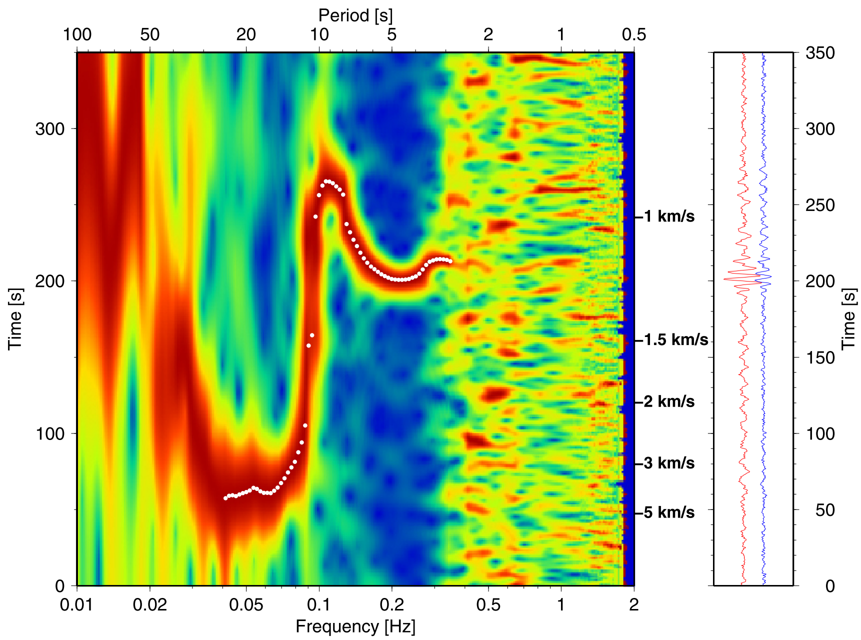

Fig. 2. Example of dispersion curve analysis (left panel) of hydrophone component seismic record (right panel) between station 01 and 11 (locations indicated in Fig. 1). Note the slight asymmetry between the causal (red) and acausal (blue) phases. The dispersion curve analysis is in the left panel (red colors indicate high, blue colors low amplitudes). Traces are normalized in every frequency/period band, travel time picks are indicated by white dots. Corresponding group velocities are indicated at the right side of the panel. A highly dispersed surface wave (Rayleigh/Scholte phases) can be identified for signal periods between 30 and 3 s. (For interpretation of the references to color in this figure, the reader is referred to the web version of this article.)

For analysis purposes we used the vertical seismometer and hydrophone component data from 22 stations which were recovered and appeared to be of good quality. Then, as a part of preprocessing stage, these data had been then restituted, decimated to 5 samples per second and split into daily segments for further processing.

3. Methods

Surface wave analysis of seismic ambient noise based investigation allows focusing primarily on crustal and uppermost mantle structures ranging from global to local scales (depending on network design), which is hard to achieve in surface wave dispersion method due to scattering and attenuation. The fundamental mode of Rayleigh waves in Green's functions between adjacent stations can be successfully extracted from sufficiently long recordings of seismic ambient noise, providing input to structural analysis with tomographic methods. Assuming that the noise sources are randomly distributed in space, cross-correlation of recordings of diffuse wave fields allow retrieving the Green's function or seismic impulse response. Most of the research and application of this technique focuses on the recovery and analysis of surface waves from ambient noise (Campillo and Paul, 2003; Shapiro et al., 2005; Schuster, 2009; Campillo and Roux, 2014). Several surveys, successfully targeting at onshore volcanoes related structures (magma chambers, volcanic deposits, volcanic edifices, calderas, etc.) had been conducted (Stankiewicz et al., 2010; Jaxybulatov et al., 2014; Zulfakriza et al., 2014; Matos et al., 2015; Shomali and Shirzad, 2015; Mordret et al., 2015; Brenguier et al., 2007; Jay et al., 2012; Masterlark et al., 2010; Spica et al., 2015). Only a few studies involving ocean bottom seismographs or amphibious seismic instrumentation exist targeting at marine volcanic structures and basins (Harmon et al., 2007; Zha et al., 2014; Corela et al., 2017) and shallow marine sediments (Mordret et al., 2013).

A combination of several methods was applied to the data to derive a final S-wave velocity model (Ryberg et al., 2016). According to Bensen et al. (2007) we whitened the spectra, applied one-bit normalization, cross-correlated data of station pairs in the frequency domain, and subsequently stacked the daily cross-correlations. The correlation function corresponds to the Green's function of seismic waves traveling from station 1 to station 2 and vice-versa. Cross-correlations at land stations are generally dominated by surface waves, since most of the background noise is assumed to be caused by surface processes. However, in the case of stations at the ocean floor, most of the noise will be created at the sea surface, within the (thick) water column and as well at the seafloor. Since we cross-correlated all vertical and all hydrophone component data individually, the surface waves we retrieved are mainly Rayleigh waves. Judging from the daily cross-correlations the noise sources appear to be stable, no strong seasonal changes of noise sources could be observed, while the spatial distribution of noise sources is non-uniform (Fig. S2). Fig. S3 shows a distance sorted plot of all obtained cross-correlations with a clearly visible fundamental mode Rayleigh wave, which in our case is actually a Scholte wave (Scholte, 1947), because of the presence of a water layer.

We determined the group velocities of the Rayleigh waves using a multiple-filter, frequency-time analysis (Dziewonski et al., 1969). Fig. 2 shows the result of the frequency-time analysis for the station pair 01–11, dominated by a fundamental mode Rayleigh wave. Group velocities had been picked manually for vertical (ZZ) and hydrophone (HH) component data cross-correlations, resulting in ∼30000 group velocity determinations in the period range from 2 to 30 s (at 84 different periods, Fig. S4) individually for the causal and acausal phases. Generally, the group velocities for both phases match well. Group velocities determined by HH and ZZ cross-correlations virtually coincide for a given station pair. We observed occasionally that for one component the signal-to-noise ratio at the lowest and/or highest signal frequencies of interest (Fig. S4) was better than for the other one. Group velocity determinations for short inter-station distances had been avoided because of the far-field approximation of the time-domain signal by requiring a minimum of three wavelengths for inter-station distance.

For each single period, the group velocities (or travel time picks of Rayleigh waves) between station pairs were used to derive group velocity maps applying the FMST (Fast Marching Surface Tomography) package (Rawlinson and Sambridge, 2005). We used an inversion grid composed of 15 by 20 cells with a cell size of ∼35 by ∼38 km. The homogeneous starting velocity model was data driven; picking outliers were removed automatically during the inversion according to Ryberg et al. (2016). Fig. S5 shows an example of the group velocity map at a period of 3.74 s.

It is well known that the water column above the OBS has a significant influence on the dispersion curves. Dispersion curves between station pairs contain information from both, the crustal and upper mantle structure and the (varying) water depth along the ray path between the stations. The 2D tomography for a selected signal period derives a 2D group velocity map by spatially "decomposing" inter-station group velocity dispersion data. The complete set of group velocity map for all signal periods can be interpreted as a set of virtual dispersion curves at every inversion grid point. Note that these virtual dispersion curves in every grid cell still contain information from both, the local subsurface structure (crust and upper mantle) and the local (grid cell specific) water depth. In the following step, we performed a search for a local velocity model by inverting the virtual dispersion curve. During this step we considered a local (grid cell specific) water depth, thus separating the influence of the water column from the crustal and upper mantle velocity structure.

The output of the group velocity tomography was a set of two-dimensional velocity maps at 84 periods. We inverted for one-dimensional velocity depth functions Vs(z) at every grid point by inverting the corresponding tomographically derived dispersion curve. The inversion of group velocity dispersion curves for Vs depth functions is highly non-unique, especially when using only fundamental mode Rayleigh wave information as in the present study. The incorporation of other surface waves (Love, higher modes, etc.) and/or body waves (receiver functions, P- and S-waves, etc.) might help to reduce the depth inversion ambiguities. Several strategies address the non-uniqueness of the depth inversion process. The inclusion of *a priori* information from other investigations (e.g. Matos et al., 2015; Stehly et al., 2009; Li et al., 2012; Shen et al., 2013) can be used to derive a background or starting models to reduce the ambiguity of the surface wave depth inversion step. Another strategy could be to investigate systematically the low dimensional model space (layer thickness and velocities) by Monte Carlo methods and Bayesian approaches (e.g. Brenguier et al., 2007; Stehly et al., 2009; Shen et al., 2013; Macquet et al., 2014). In our study we used the code *surf96* (Herrmann and Ammon, 2004), which is based on an iterative linearized least-square inversion. This inversion technique needs a reasonable starting velocity model. Instead of using an *a priori* model we determined a data driven starting velocity model. We inverted the averaged dispersion curve (mean group velocity for every period) with a large number (>20000) of randomly chosen starting models (random layer thickness from 0.5 to several km, and velocity values covering the range of crustal and uppermost mantle rocks: Vs from 0.1 to 4.5 km/s, assuming a V_p/V_s ratio and density according to Brocher (2005). The 10000 best fitting models were averaged and used as a reasonable starting model with 16 layers (Figs. S7 and S8). We then inverted for 1D structure in every grid cell to construct a 3D model. The actual depth inversion was done at every grid cell assuming the local average ocean depth (ETOPO2) and local tomographically derived dispersion curve. Considering the local water depth is crucial, since the water column above the inversion cell has a significant impact on the inversion result.

To assess the resolving power of the imaging technique we performed checkerboard tests to evaluate the spatial resolution. We tested 2D checkerboards (20% velocity perturbations for every 84 signal periods, ∼80 by ∼80 km). This recovery test was designed to test mainly the horizontal resolution of structural features. By combining the two inversion techniques (2D tomography and depth inversion) to the checkerboard data set we are also able to evaluate the limited depth resolution introduced by the depth inversion step. Although this is not a complete 3D checkerboard test, necessary to correctly estimate spatial resolution (laterally and vertically), we generally found a good spatial recovery at shallower depth, degrading somewhat at depth (Fig. S9). The checkerboard recovery test was also used to determine the regularization parameters (with optimal damping $\varepsilon = 5$ and smoothing $\eta = 1$, notation as used in FMST, Rawlinson and Sambridge, 2005). The choice of these parameters appeared to have only a small impact on the final inversion result.

4. Results

We present four depth slices (Fig. 3) for our 3D S-wave model at 4, 5.5, 10.5 and 14.5 km depths. To enhance structural features we show the velocity perturbation with respect to the mean at that depth, the latter coinciding with the velocity value of the starting model. The 4 km-depth slice (mostly just below sea bottom) is dominated by a circular high velocity zone of ∼100 km diameter, centered on the Tristan da Cunha Island. The velocity values outside this high velocity anomaly are significantly lower, except in the southwestern part of the study region. At greater depths (∼5.5 km), the shape of the velocity anomaly still persists, but the relative velocity contrast is reduced. At depths of ∼10.5 km, we observe decreased velocities directly beneath the islands, surrounded mainly in the NE by higher velocities. Towards the SW we also observe low velocities at 10.5 km depth. The last depth slice at ∼15 km does not show/resolve any significant velocity variations.

Fig. 4 shows a latitudinal and a longitudinal vertical depth slice through the 3D model, centered on Tristan da Cunha (Fig. S10 shows the same slices with relative velocity color scale). The shallow submarine part of the volcanic islands (the flanks) down to 3 km model depth is characterized by very low S wave velocities not exceeding 1.5 km/s (see also Figs. S6, S7), similar to those of 4 km depth slice of Fig. 3. Off the volcano region, a low velocity layer is observed down to ∼5 km model depth (1 to 1.5 km below the seafloor) with velocities between 1.5 and 1.8 km/s. Again, a shallow (at around 5 km depth) high velocity body (Vs ∼2.5 km/s, 5 km depth slice Fig. 3) exists beneath the islands. Deeper below the island, at 8 km model depth (down to ∼13 km, compare to 10.5 km depth slice Fig. 3), anomalous low velocities of about 3 km/s are present, surrounded by typical mantle velocities (>4 km/s). Fig. 4(a) also illustrates high velocities in the uppermost mantle beneath the Tristan da Cunha Fracture Zone, but relatively low velocities further south towards the Speedwell-Hercules Seamount Chain.

Although the starting model was carefully chosen (Fig. S7), the absolute velocity values of our model still depend significantly on the starting model. Even further, given the nature and sensitivity of Rayleigh waves with depth (depth dependent smoothing), no sharp discontinuities (Moho) and, thus, no reliable absolute crustal thicknesses can be determined. This might hinder a direct comparison of absolute velocity and crustal thickness values of our 3D model with seismic velocities otherwise derived.

5. Interpretation

The oceanic crust and underlying lithosphere in the study area was formed at the mid-Atlantic ridge between 30–10 Ma (Müller et al., 2008). If a strong mantle plume contributed to the melting

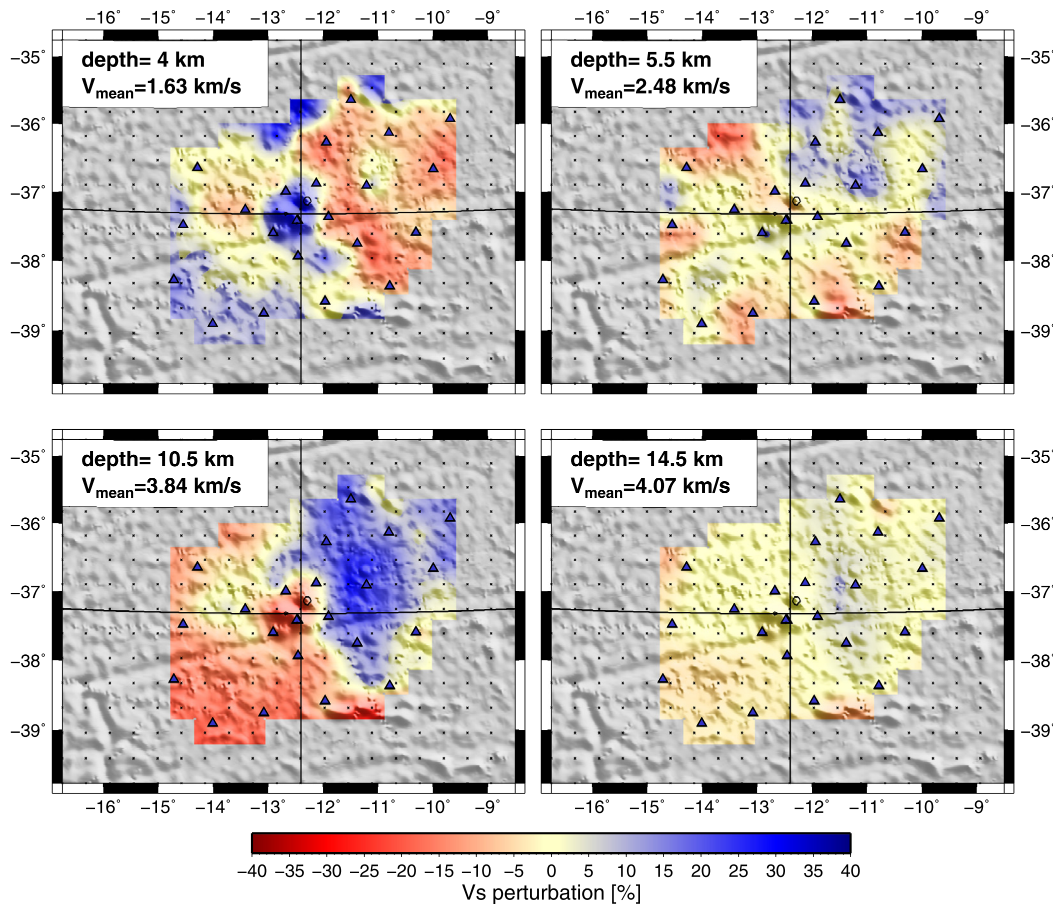

Fig. 3. Horizontal depth slices (relative scale) through final Vs model. Note the high and low velocity anomalies at the islands of Tristan da Cunha. Small dots indicate the inversion cells centers, black triangles show the seismic network. Depths (below sea level) and average velocities are shown. Lines indicate position of slices shown in Fig. 4.

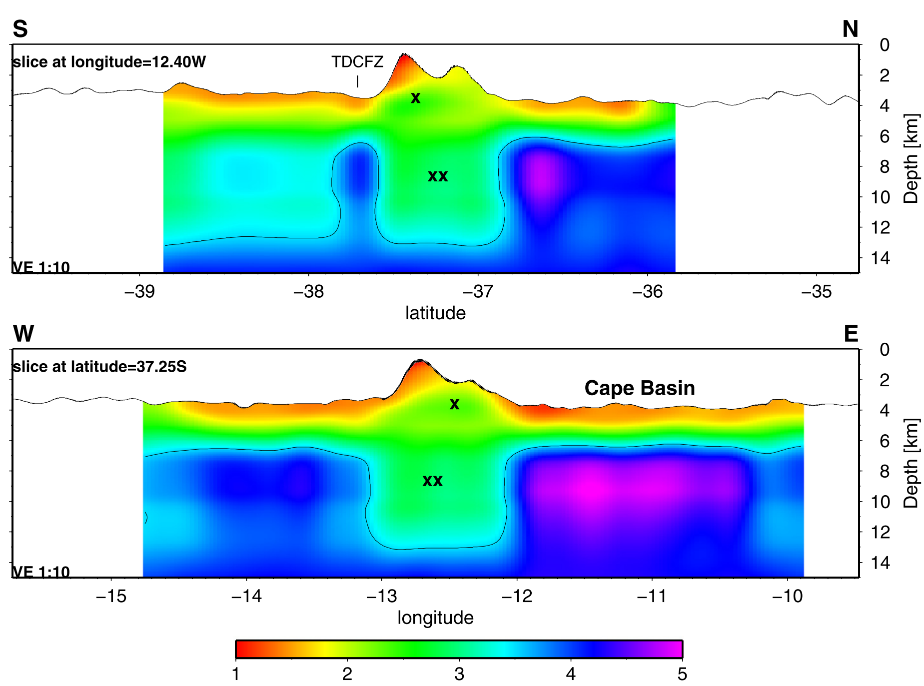

Fig. 4. Vertical cross sections (absolute scale) through final Vs model, centered at Tristan da Cunha. Low to very low velocities are present in the shallowest part of the model. A high velocity body just below the island reaches down to 5 km depth. The deeper (mantle) part below TDC is characterized by anomalous low velocities. Location of the slices are marked in Fig. 3. The high velocity region marked with x is interpreted as solidified basaltic intrusions. The deeper reaching low velocity region marked with xx might represent partially molten magmas.

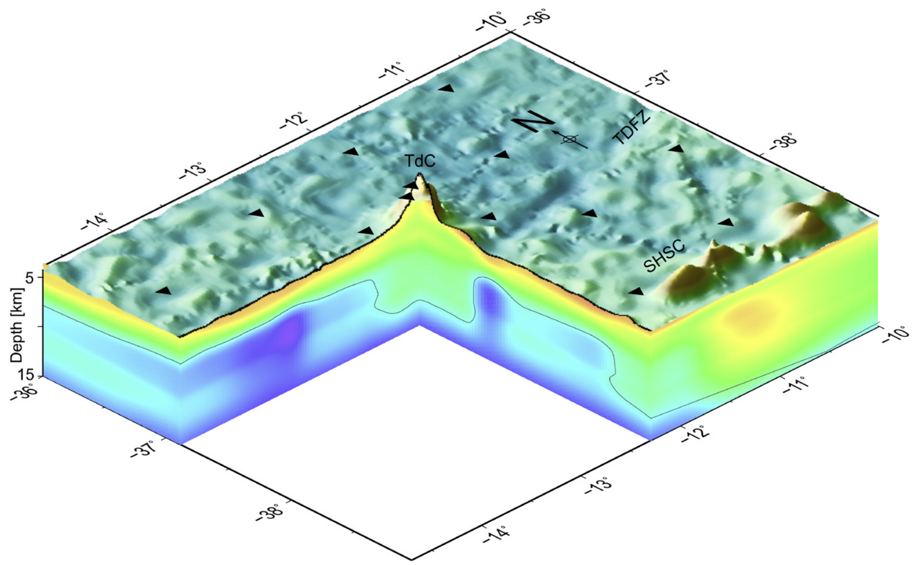

Fig. 5. 3D model view from SW towards Tristan da Cunha (TdC). The low velocities beneath the islands are clearly illustrated as well as the thin oceanic crust in the surrounding. Low velocities beneath the Speedwell-Hercules Seamount Chain (SHSC) might be real but are not well resolved at the periphery of the seismological network. The Tristan-da-Cunha Fracture Zone (TDCFZ) seems to be associated with increased (normal) S wave velocities in the uppermost mantle.

along the mid-ocean ridge, we should expect thicker than normal oceanic crust over all the study area (see White et al., 1992). Also we would expect additional hotspot material was added to the lower crust and therefore thickened the pre-existing oceanic crust above the potential location of the mantle plume, which have been active in our study area at least during the last ∼0.5–1 Ma, the lifetime of Tristan da Cunha (O'Connor and le Roex, 1992).

Though we technically can interpret the crustal thickness only qualitatively due to missing depth sensitivity of the method, we observe a relatively thin oceanic crust in the study area. The thickness of <5 km is comparable with results from a receiver function study (Geissler et al., in press) within the uncertainties of both methods. Similar results are reported from an active seismic experiment northeast of our study area across the Walvis Ridge at 4°W (Jokat and Reents, 2017). In the Cape Basin adjacent to the aseismic ridge only 4 km thick crust on average has been detected. The internal structure and relative thickness of the oceanic crust do not vary dramatically in our study area, except for that areas overprinted by young volcanic activity in close vicinity to the islands and seamounts. That means that a potential mantle plume did not strongly enhance the melting along the mid-oceanic ridge by adding heat to the system.

We interpret the uppermost crust (first few km) with its relatively low velocities around the island as volcanic effusiva and volcanoclastic sediments, deposited at and along the flanks of the volcanic island. The shallow low velocity layer at the top of the crust surrounding the islands might represent the typical uppermost oceanic crustal layer (Christensen and Salisbury, 1975) consisting of pillow basalts with only a thin sedimentary veneer. There are no major differences between the regions north and south of Tristan da Cunha (NS direction) in terms of crustal thickness or internal crustal structure, indicating comparable melting regimes (potential temperature) below the mid-ocean ridge segment axes (White et al., 1992). The relatively high velocity anomaly located at 4.5–5.0 km depth just beneath the volcanic edifices (marked with x in Figs. 4 and S10) might be solidified basaltic intrusions.

We interpret the well-developed almost vertical structure of anomalous low velocities (marked with xx in Figs. 4 and S10) below the archipelago starting at 7 km depth and reaching at least down to ∼13 km as crystallized and partially molten magmas emplaced close to the pre-existing oceanic Moho (Fig. 5), in accordance with petrological data from Weit et al. (2016). The apparent absence of expected, deep reaching magmatic feeding structures at shallower depth could be easily explained by the expected smaller size of the feeding pathways through the volcanic structure, which is beyond the resolution of our applied method. Interestingly the observed major velocity anomaly beneath the volcanic edifices of Tristan da Cunha is laterally very sharp (Fig. 5). This indicates that the magmatic modification of the lithosphere is restricted to an area of about 100 km in diameter, which might have been stable in position over the time of formation of Tristan da Cunha (0.5–1 Ma, O'Connor and le Roex, 1992). There is a minor slow velocity anomaly in the uppermost mantle in the vicinity of the Speedwell-Hercules seamount chain (see Fig. 5). This might be again an indication of the magmatic overprint (intrusions) within the uppermost mantle beneath those underwater volcanoes comparable to Tristan da Cunha but smaller in size and volume.

As it can be seen from Fig. 4 we observe higher shear wave velocities in the uppermost mantle to the North and East of Tristan da Cunha (see also Figs. S6 and S7). This area is also characterized by an anomalously deeper seafloor (Baba et al., 2016). In contrast we found the above-mentioned low-velocity anomalies beneath the islands and seamounts, but also relatively low velocities in the uppermost mantle in the SW part of the study area (Figs. S6 and S7). Schloemer et al. (2017) image in our research area a low P-wave velocity conduit in the upper mantle in 100 to >250 km depth, which they interpret as the expression of a weak mantle plume. This area of reduced seismic velocities might be an indication that the uppermost (shallow lithospheric) mantle shows the very first signs of magmatic overprinting without major volcanic centers at the seafloor. In this area there are not yet major seamounts reported, which can be identified by satellite derived bathymetry. However, high-resolution ship-born bathymetric data provide first signs of intra-plate volcanism (Geissler et al., pers. commun.). Alternatively, slower S wave velocities in the SW of Tristan da Cunha might partly still reflect the different age and therefore temperature of the oceanic lithosphere north and south of the Tristan da Cunha Fracture Zone (TDCFZ). Since our data images only the shallowest part of the oceanic lithosphere, it is not conclusive about seismic/electromagnetic anomalies and related geodynamic processes in the asthenosphere or the deeper lithosphere. Just from this ambient seismic noise study we cannot contribute to the debate on the existence of a weak mantle plume in close vicinity to Tristan da Cunha and its potential interaction with the overlying oceanic lithosphere (Baba et al., 2016; Schloemer et al., 2017).

Our results displayed in Figs. 4 and 5 (see also Figs. S6 and S7) clearly illustrate that the Tristan da Cunha Fracture Zone (TDCFZ) is not only a topographical feature but can be traced seismically into the uppermost mantle. Even if it seems obvious that transform faults and fracture zones are lithosphere-scale features, the deep (upper mantle) structure of fracture zones is still underexplored. Crustal scale studies and geological sampling provided sufficient evidence that many of the major transform and fracture zones are underlain by thin crust, ultramafic rocks, serpentinites and mylonites (e.g., Detrick and Purdy, 1980; White et al., 1984; Maia et al., 2016 and references therein). Transform faults and therefore also fracture zones are assumed to be cooler than the adjacent plate segments (e.g., Morgan and Forsyth, 1988), thus they should have higher uppermost mantle seismic S wave velocities compared to the hotter segment centers.

The uppermost mantle seismic velocities beneath the western TDCFZ seem to be normal in comparison to the decreased velocities beneath Tristan da Cunha, the Speedwell-Hercules Seamount chain and the western part of the southern plate segment (see Figs. S11, S12). For the later one it is difficult to differentiate between the thermal effects of the cooling plate segments and any recent magmatic overprint by a potentially underlying mantle plume. East of Tristan da Cunha (12°W), the TDCFZ is not visible as a strong uppermost mantle feature anymore in our tomography sections, but still higher uppermost mantle seismic velocities are imaged towards the northern (older) segment.

6. Conclusions

We derived a 3D S wave velocity model around the Tristan da Cunha archipelago by analyzing ambient seismic noise. The crustal and upper mantle structure surrounding Tristan da Cunha Island is surprisingly homogeneous. We map relatively thin oceanic crust (<5 km) north and south of the Tristan da Cunha Fracture Zone, keeping in mind that the depth and velocity resolving capabilities of Rayleigh waves alone (with only fundamental mode) is limited. We take this overall thin oceanic (magmatic) crust as evidence that there is no major contribution of a potential mantle plume and melt anomaly to the crustal production at the nearby mid-ocean ridge.

The velocity model shows a spatially limited S-wave velocity anomaly centered at the Tristan da Cunha Island. It is characterized by shallow high velocities interpreted as solidified magmatic material and a deeper reaching root of low velocity material. We interpret these velocity structures as indicative for a magma feeding system mainly beneath the active volcanic archipelago. There is no major magmatic thickening of the oceanic crust and uppermost mantle by the Tristan hotspot to the North and East of the islands. Low velocities are also mapped beneath the nearby Speedwell-Hercules Seamount Chain and beneath the SW part of the seismological network. This indicates the existence of a feeding system also beneath the seamounts and a potential initial magmatic overprint to the SW of Tristan da Cunha above the potential location of a mantle plume conduit in the deeper upper mantle.

The Tristan da Cunha Fracture Zone can be distinguished by its velocities in its western part, where we have the anomalous seismic low velocities to the north and south, giving evidence for only minor magmatic overprinting along the fracture zone itself.

Acknowledgements

This work was supported by the German Research Foundation (DFG) grant GE 1783/4-1/2 as part of the Priority Program SPP1375. Additional support was provided by the Alfred Wegener Institute Bremerhaven. Instruments were provided by "Deutscher Geräte-Pool für Amphibische Seismologie (DEPAS)" at Alfred Wegener Institute Bremerhaven and Deutsches GeoForschungsZentrum GFZ Potsdam. We thank the captain Ralf Schmidt, the crew of R/V Maria S. Merian and the Scientific Parties of cruises MSM20/2 and MSM24 as well as the people on Tristan da Cunha for the professional and friendly support. Figures were prepared using the Generic Mapping Tool GMT (Wessel and Smith, 1995; Wessel and Smith, 1998). Raw data are archived at Alfred Wegener Institute by the Geophysics Section. Data requests should be made to Wolfram Geissler (Wolfram.Geissler@awi.de) or Mechita Schmidt-Aursch (Mechita.Schmidt-Aursch@awi.de). We would like to thank the two anonymous reviewers who provided comments that greatly improved the manuscript.

Appendix A. Supplementary material

Supplementary material related to this article can be found online at http://dx.doi.org/10.1016/j.epsl.2017.04.049.

References

Baba, K., Chen, J., Sommer, Ma., Utada, H., Geissler, W.H., Jokat, W., Jegen, M., 2016. Marine magnetotellurics imaged no distinct plume beneath the Tristan da Cunha hotspot in the southern Atlantic Ocean. Tectonophysics. http://dx.doi.org/10.1016/j.tecto.2016.09.033.

Bensen, G.D., Ritzwoller, M.H., Barmin, M.P., Levshin, A.L., Lin, F., Moschetti, M.P., Shapiro, N.M., Yang, Y., 2007. Processing seismic ambient noise data to obtain reliable broadband surface wave dispersion measurements. Geophys. J. Int. 169, 1239–1260. http://dx.doi.org/10.1111/j.1365-246X.2007.03374.x.

Brenguier, F., Shapiro, N.M., Campillo, M., Nercessian, A., Ferrazzini, V., 2007. 3-D surface wave tomography of the Piton de la Fournaise volcano using seismic noise correlations. Geophys. Res. Lett. 34, L02305.

Brocher, T.M., 2005. Empirical relations between elastic wavespeeds and density in the Earth's crust. Bull. Seismol. Soc. Am. 95 (6), 2081–2092. http://dx.doi.org/10.1785/0120050077.

Campillo, M., Paul, A., 2003. Long-range correlations in the diffuse seismic coda. Science 299, 547–549.

Corela, C., Silveira, G., Matias, L., Schimmel, M., Geissler, W.H., 2017. Ambient seismic noise tomography of SW Iberia integrating seafloor- and land-based data. Tectonophysics 700–701, 131–149. http://dx.doi.org/10.1016/j.tecto.2017.02.012.

Campillo, M., Roux, P., 2014. Seismic imaging and monitoring with ambient noise correlations. In: Romanowicz, B., Dziewonski, A. (Eds.), Treatise on Geophysics, second ed. 1. Elsevier, Amsterdam, pp. 256–271.

Courtillot, V., Davaille, A., Besse, J., Stock, J., 2003. Three distinct types of hotspots in the Earth's mantle. Earth Planet. Sci. Lett. 205, 295–308. http://dx.doi.org/10.1016/S0012-821X(02)01048-8.

Christensen, N.I., Salisbury, M.H., 1975. Structure and constitution of the lower oceanic crust. Rev. Geophys. 13 (1), 57–86. http://dx.doi.org/10.1029/RG013i001p00057.

Detrick, R.S., Purdy, G.M., 1980. The crustal structure of the kane fracture zone from seismic refraction studies. J. Geophys. Res., Solid Earth 85 (B7), 3759–3777. http://dx.doi.org/10.1029/JB085iB07p03759.

Dziewonski, A., Bloch, S., Landisman, M., 1969. A technique for the analysis of transient seismic signals. Bull. Seismol. Soc. Am. 59 (1), 427–444.

Fromm, T., Planert, L., Jokat, W., Ryberg, T., Behrmann, J.H., Weber, M., Haberland, C., 2015. South Atlantic opening: a plume-induced breakup? Geology 43 (10), 931–934.

Geissler, W.H., Jokat, W., Jegen, M., Baba, K., in press. Thickness of the oceanic crust and the mantle transition zone in the vicinity of the Tristan da Cunha hot spot estimated from ocean-bottom and ocean-island seismometer receiver functions. Tectonophysics. http://dx.doi.org/10.1016/j.tecto.2016.12.013.

Harmon, N., Forsyth, D., Webb, S., 2007. Using ambient seismic noise to determine short-period phase velocities and shallow shear velocities in young oceanic lithosphere. Bull. Seismol. Soc. Am. 97 (6), 2009–2023. http://dx.doi.org/10.1785/0120070050.

Herrmann, R.B., Ammon, C.J., 2004. Surface Waves, Receiver Functions and Crustal Structure. Computer Programs in Seismology, Version 3.30. Saint Louis University. http://www.eas.slu.edu/People/RBHerrmann/CPS330.html.

Hicks, A., Barclay, J., Mark, D.F., Loughlin, S., 2012. Tristan da Cunha: constraining eruptive behavior using the $^{40}Ar/^{39}Ar$ dating technique. Geology 40, 723–726.

Jaxybulatov, K., Shapiro, N.M., Koulakov, I., Mordret, A., Landes, M., Sens-Schönfelder, C., 2014. A large magmatic sill complex beneath the Toba caldera. Science 346 (6209), 617–619.

Jay, J.A., Pritchard, M.E., West, M.E., Christensen, D., Haney, M., Minaya, E., Sunagua, M., McNutt, S.R., Zabala, M., 2012. Shallow seismicity, triggered seismicity, and ambient noise tomography at the long-dormant Uturuncu Volcano, Bolivia. Bull. Volcanol. 74 (4), 817–837. http://dx.doi.org/10.1007/s00445-011-0568-7.

Jokat, W., Reents, S., 2017. Hotspot volcanism in the southern South Atlantic: geophysical constraints on the evolution of the southern Walvis Ridge and the Discovery Seamounts. Tectonophysics. http://dx.doi.org/10.1016/j.tecto.2016.12.011.

Li, H., Li, S., Song, X.D., Gong, M., Li, X., Jia, J., 2012. Crustal and uppermost mantle velocity structure beneath northwestern China from ambient noise tomography. Geophys. J. Int. 188, 131–143.

Macquet, M., Paul, A., Pedersen, H.A., Villasenor, A., Chevrot, S., Sylvander, M., Wolyniec, D., 2014. Ambient noise tomography of the Pyrenees and the surrounding regions: inversion for a 3-D Vs model in the presence of a very heterogeneous crust. Geophys. J. Int. 199 (1), 402.

Maia, M., et al., 2016. Extreme mantle uplift and exhumation along a transpressive transform fault. Nat. Geosci. http://dx.doi.org/10.1038/ngeo2759. Advance online publication.

Masterlark, T., Haney, M., Dickinson, H., Fournier, T., Searcy, C., 2010. Rheologic and structural controls on the deformation of Okmok volcano, Alaska: FEMs, InSAR, and ambient noise tomography. J. Geophys. Res. 115 (B2), B02409. http://dx.doi.org/10.1029/2009JB006324.

Matos, C., Siveira, G., Matias, L., Caldeira, R., Ribeiro, M.L., Dias, N.A., Krüger, F., Bento dos Santos, T., 2015. Upper crustal structure of Madeira Island revealed from ambient noise tomography. J. Volcanol. Geotherm. Res. 298, 136–145.

Mordret, A., Rivet, D., Landès, M., Shapiro, N.M., 2015. Three-dimensional shear velocity anisotropic model of Piton de la Fournaise Volcano (La Réunion Island) from ambient seismic noise. J. Geophys. Res., Solid Earth 120, 406–427. http://dx.doi.org/10.1002/2014JB011654.

Mordret, A., Shapiro, N.M., Singh, S.S., Roux, P., Barkved, O.I., 2013. Helmholtz tomography of ambient noise surface wave data to estimate Scholte wave phase velocity at Valhall Life of the field. Geophysics 78 (2), WA99–WA109. http://dx.doi.org/10.1190/GEO2012-0303.1.

Morgan, W.J., 1971. Convection plumes in the lower mantle. Nature 230, 42–43. http://dx.doi.org/10.1038/230042a0.

Morgan, J.P., Forsyth, D.W., 1988. Three-dimensional flow and temperature perturbations due to a transform offset: effects on oceanic crustal and upper mantle structure. J. Geophys. Res., Solid Earth 93 (B4), 2955–2966. http://dx.doi.org/10.1029/JB093iB04p02955.

Müller, R.D., Sdrolias, M., Gaina, C., Roest, W.R., 2008. Age, spreading rates and spreading symmetry of the world's ocean crust. Geochem. Geophys. Geosyst. 9, Q04006. http://dx.doi.org/10.1029/2007GC001743.

O'Connor, J.M., Duncan, R.A., 1990. Evolution of the Walvis Ridge-Rio Grande Rise Hot Spot System: implications for African and South American Plate motions over plumes. J. Geophys. Res., Solid Earth 95 (B11), 17475–17502. http://dx.doi.org/10.1029/JB095iB11p17475.

O'Connor, J.M., le Roex, A.P., 1992. South Atlantic hot spot-plume systems: 1. Distribution of volcanism in time and space. Earth Planet. Sci. Lett. 113 (3), 343–364.

O'Mongain, A., Ottemoller, L., Brian, B., Galloway, D., Booth, D., 2007. Seismic activity associated with a probable submarine eruption near Tristan da Cunha, July 2004–July 2006. Seismol. Res. Lett. 78 (3), 375–382.

Rawlinson, N., Sambridge, M., 2005. The fast marching method: an effective tool for tomographic imaging and tracking multiple phases in complex layered media. Explor. Geophys. 36, 341–350.

Rohde, J.K., van den Bogaard, P., Hoernle, K., Hauff, F., Werner, R., 2013. Evidence for an age progression along the Tristan–Gough volcanic track from new $^{40}Ar/^{39}Ar$ ages on phenocryst phases. Tectonophysics 604, 60–71. http://dx.doi.org/10.1016/j.tecto.2012.08.026.

Ryberg, T., Haberland, Ch., Haberlau, T., Weber, M.H., Bauer, K., Behrmann, J.H., Jokat, W., 2015. Crustal structure of northwest Namibia: evidence for plume-rift-continent interaction. Geology. http://dx.doi.org/10.1130/G36768.1.

Ryberg, T., Muksin, U., Bauer, K., 2016. Ambient seismic noise tomography reveals a hidden caldera and its relation to the Tarutung pull-apart basin at the Sumatran Fault Zone, Indonesia. J. Volcanol. Geotherm. Res. http://dx.doi.org/10.1016/j.jvolgeores.2016.04.035.

Schilling, J.G., Thompson, G., Kingsley, R., Humphris, S., 1985. Hotspot-migrating ridge interaction in the South Atlantic. Nature 313 (5999), 187–191.

Schloemer, A., Geissler, W.H., Jokat, W., Jegen, M., 2017. Hunting for the Tristan Mantle Plume – an upper mantle tomography around the volcanic island of Tristan da Cunha. Earth Planet. Sci. Lett. 462, 122–131. http://dx.doi.org/10.1016/j.epsl.2016.12.028.

Scholte, J.G., 1947. The range and existence of Rayleigh and Stoneley waves. Geophys. J. Int. 5, 120–126. http://dx.doi.org/10.1111/j.1365-246X.1947.tb00347.x.

Shapiro, N.M., Campillo, M., Stehly, L., Ritzwoller, M.H., 2005. High-resolution surface wave tomography from ambient seismic noise. Science 307, 1615–1618.

Shen, W., Ritzwoller, M.H., Schulte-Pelkum, V., 2013. A 3-D model of the crust and the uppermost mantle beneath the Central and Western US by joint inversion of receiver functions and surface wave dispersion. J. Geophys. Res. 118, 262–276.

Schuster, G.T., 2009. Seismic Interferometry. Cambridge University Press.

Shomali, Z.H., Shirzad, T., 2015. Crustal structure of Damavand volcano, Iran, from ambient noise and earthquake tomography. J. Seismol. 19, 191–200.

Spica, Z., Legrand, D., Iglesias, A., Walter, T.R., Heimann, S., Dahm, T., Froger, J.-L., Rémy, D., Bonvalot, S., West, M., Pardo, M., 2015. Hydrothermal and magmatic reservoirs at Lazufre volcanic area, revealed by a high-resolution seismic noise tomography. Earth Planet. Sci. Lett. 421, 27–38. http://dx.doi.org/10.1016/j.epsl.2015.03.042.

Stankiewicz, J., Ryberg, T., Haberland, C., Fauzi, N., Natawidjaja, D., 2010. Lake Toba volcano magma chamber imaged by ambient seismic noise tomography. Geophys. Res. Lett. 37, L17306.

Stehly, L., Fry, B., Campillo, M., Shapiro, N.M., Guilbert, J., Boschi, L., Giardini, D., 2009. Tomography of the Alpine region from observations of seismic ambient noise. Geophys. J. Int. 178 (1), 338–350. http://dx.doi.org/10.1111/j.1365-246X.2009.04132.x.

Weit, A., Trumbull, R.B., Keiding, J.K., Geissler, W.H., Gibson, S.A., Veksler, I.V., 2016. The magmatic system beneath the Tristan da Cunha Island: insights from thermobarometry, melting models and geophysics. Tectonophysics. http://dx.doi.org/10.1016/j.tecto.2016.08.010.

Wessel, P., Smith, W., 1995. New version of the Generic Mapping Tools released. Suppl. to Eos Trans. AGU 76, 329.

Wessel, P., Smith, W., 1998. New, improved version of the Generic Mapping Tool released. Suppl. to Eos Trans. AGU 79, 579.

White, R.S., Detrick, R.S., Sinha, M.C., Cormier, M.H., 1984. Anomalous seismic crustal structure of oceanic fracture zones. Geophys. J. R. Astron. Soc. 79 (3), 779–798. http://dx.doi.org/10.1111/j.1365-246X.1984.tb02868.x.

White, R.S., McKenzie, D., O'Nions, R.K., 1992. Oceanic crustal thickness from seismic measurements and rare earth element inversions. J. Geophys. Res., Solid Earth 97 (B13), 19683–19715. http://dx.doi.org/10.1029/92JB01749.

Zha, Y., Webb, S.C., Wei, S.S., Wiens, D.A., Blackman, D.K., Menke, W.H., Dunn, R.A., Conders, J.A., 2014. Upper mantle shear velocity structure beneath the Eastern Lau Spreading Center from OBS ambient noise tomography. Earth Planet. Sci. Lett. 408 (0), 194–206. http://dx.doi.org/10.1016/j.epsl.2014.10.019.

Zulfakriza, Z., Saygin, E., Cummins, P.R., Widiyantoro, S., Nugraha, A.D., Lühr, B.G., Bodin, T., 2014. Upper Crustal Structure of Central Java, Indonesia, from Transdimensional Seismic Ambient Noise Tomography. Geophys. J. Int. 197, 630–635. http://dx.doi.org/10.1093/gji/ggu016.